

Singlet-triplet mixed state in spin-orbital-parity coupled superconductors

Tsz Fung Heung* and Yip Chun Wong*

Department of Physics, Hong Kong University of Science and Technology, Clear Water Bay, Hong Kong, China

(Dated: November 5, 2024)

Unlike noncentrosymmetric superconductors, the effects of spin singlet- and spin triplet-pairing mixing in centrosymmetric superconductors remain ambiguous. Recently, it was experimentally demonstrated that an anisotropically enhanced in-plane critical fields beyond Pauli limit would be induced by the coupling of spin, orbit and parity (p -, d -orbitals) degrees of freedom in centrosymmetric transition metal dichalcogenides, which is called as spin-orbit-parity coupled (SOPC) superconductors. In this work, we show that the SOPC would induce a strong spin-singlet and spin-triplet pairing mixing near the topological band inversion in this system. Moreover, we find that the presence of such mixing provides a close explanation of the observed the in-plane upper critical fields B_{c2} in terms of both the enhancement and anisotropy. We also propose measuring the equal-spin Andreev reflection between 2M-WS₂ and a ferromagnetic (FM) lead to detect the spin-triplet pairing in 2M-WS₂. Our work paves a way to study the spin-singlet and spin-triplet pairing in centrosymmetric superconductors with strong spin-orbital parity coupling.

Introduction.— A superconductor can be classified into noncentrosymmetric and centrosymmetric superconductors according to its crystal symmetry. In a noncentrosymmetric superconductor, the spin-singlet and spin-triplet pairing would generally mix with each other in the presence of strong spin-orbit coupling $\mathbf{g}(\mathbf{k}) \cdot \boldsymbol{\sigma}$ (\mathbf{k} is momentum, σ_j is Pauli matrices) [1]. One important consequence of this pairing mixing is to enhance the upper critical fields of noncentrosymmetric superconductors [2, 3], which have been well explored in some noncentrosymmetric superconductors, such as heavy fermion superconductors [4], Ising superconductor [5–15]. For centrosymmetric superconductors, due to the combination of both time-reversal symmetry and inversion symmetry, the usual spin strong spin-orbit coupling $\mathbf{g}(\mathbf{k}) \cdot \boldsymbol{\sigma}$ vanishes. As a result, the spin-singlet and spin-triplet pairing mixing are often overlooked in centrosymmetric superconductors.

In recent years, several centrosymmetric superconducting thin films with in-plane upper critical fields beyond Pauli limit (B_p) are seen in the experiments [16–21]. Notably, a large class of them are represented by various centrosymmetric transition metal dichalcogenides thin film, the monolayer of which are predicted to be a two-dimensional quantum spin Hall insulator [22–26], including 1T'-WTe₂ [16, 17], 2M-WS₂ [18], 1T'-WS₂[19]. Specifically, in the year 2018, centrosymmetric monolayer 1T'-WTe₂ was reported to be superconducting upon electrograting while the in-plane B_{c2} is one to three times B_p [16, 17]. Due to the presence of inversion symmetry, the spin-orbit coupling term that involves only spin and momentum, which is widely used to explain such enhancement in noncentrosymmetric superconductors, is not allowed in 1T'-WTe₂. Hence, another intrinsic mechanism behind the observed enhancement of B_{c2} was pointed out in Ref. [27]. It shows that the spin-orbit-parity coupling that involves the coupling the spin, orbit and parity degrees of freedom in this system would

renormalize the spin susceptibility and an anisotropic B_{c2} higher than the Pauli limit is predicted. This prediction is clearly demonstrated in the centrosymmetric superconducting 2M-WS₂ thin film recently [18], which exhibits the same structure 1T'-structure in monolayer but displays a distinct stacking along z -axis. Notably, similar anisotropically enhanced B_{c2} beyond B_p has also been seen in newly fabricated centrosymmetric 1T'-WS₂ thin film [19], which could be also explained in terms of SOPC. Given these experimental progresses, a study of whether the SOPC would induce spin-singlet and spin-triplet pairing mixing in these centrosymmetric superconductors would be highly desirable. Also, how this pairing mixing would affect the B_{c2} is also an interesting question.

In this work, using a model that captures the realistic bands of centrosymmetric TMD, we study the spin-singlet and spin-triplet pairing mixing induced by the strong SOPC in centrosymmetric superconductors. We first show that due to the presence of SOPC, the inter-orbital spin triplet pairing correlation would be non-zero. Next, we classify the possible pairings according to the irreducible representation of the point group symmetry. Importantly, we find that the trivial A_g representation contains both intra-orbital spin-singlet and inter-orbital spin-triplet pairing. As a result, a mixing between them is possible. Then, we calculate the superconducting phase diagram involving these two pairings, which shows a clear mixing region. Moreover, by calculating the superconducting pairing susceptibility at different SOPC strength, we find that the mixing strength is enhanced with the SOPC strength. Finally, we discuss the possible connection to the experiment by showing the in-plane B_{c2} with and without spin-singlet and spin-triplet pairing mixing. We find the pairing mixing helps to enhance both the magnitude and anisotropy of the B_{c2} , which provides a close fitting of the B_{c2} measured by the experiment. We also find that when a ferromagnetic lead is attached

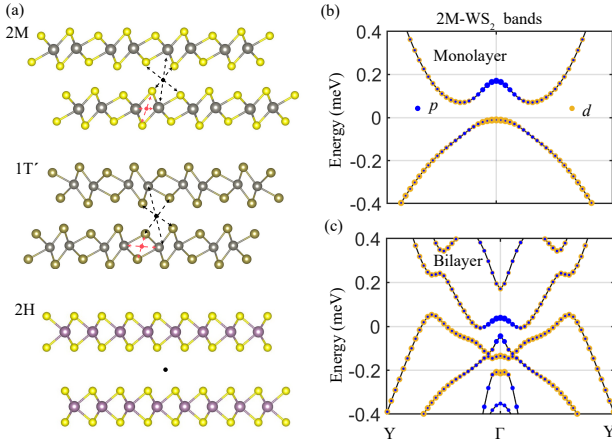


FIG. 1. (a) shows bilayer transition metal dichalcogenides with 2M-, 1T', 2H-structures, respectively. The bilayer inversion center and monolayer layer inversion center are highlighted as black and red dots, respectively. (b) and (c) show the first-principle calculated band structures of a monolayer and bilayer 2M-WS₂, respectively. The projected *d* states for the tungsten atoms and *p* states for the sulfur atoms are shown.

to 2M-WS₂, the tunneling amplitude is anisotropic due to equal-spin Andreev reflection, suggesting the existence of spin-triplet pairing in 2M-WS₂.

Model.— We first present a model which describes a centrosymmetric superconductor with strong SOPC. This model is motivated by the recent finding of superconductivity in centrosymmetric superconducting 2M-WS₂, 1T'-WTe₂ thin film. An illustration of these crystal structures is depicted in Fig. 1(a), which shows a bilayer structure of them. It can be seen that both the monolayer and bilayer 1T'- and 2M-structure are centrosymmetric (the inversion center are highlighted as red and black dot, respectively). It is distinct from the notable 2H-structure, in which although even layers are centrosymmetric but is always locally noncentrosymmetric within each layer (see bottom panel of Fig. 1(a)).

Let us first model the monolayer, which is identical for 2M- and 1T'-structure and the bands are topological [22]. The states near Fermi energy in this case are contributed by a topological band inversion between a *p*-orbital dominant band and a *d*-orbital dominant band. As an illustration of this topological band inversion, the monolayer 2M-WS₂ energy bands obtained from first principle calculation is shown in Fig. 1(b). To describe these bands, a four-band $\mathbf{k} \cdot \mathbf{p}$ Hamiltonian dedicated by the point symmetry C_{2h} to describe normal states is written as [18, 27]

$$H_0(\mathbf{k}) = \epsilon_{\mathbf{k}} + \mathcal{M}_{\mathbf{k}} s_z + v k_x s_y + (A_x k_x s_x \sigma_y + A_y k_y s_x \sigma_x + A_z k_y s_x \sigma_z) + \frac{1}{2} g_s u_B \mathbf{B} \cdot \boldsymbol{\sigma} \quad (1)$$

Here, *s* are Pauli matrices operating on (*p*, *d*) orbitals, σ are Pauli matrices operating on spin space. $\epsilon_{\mathbf{k}} = t_{0x} k_x^2 + t_{0y} k_y^2 + t_{2x} k_x^4 + t_{2y} k_y^4 - \mu$, $M(\mathbf{k}) = -\delta + m_{0x} k_x^2 +$

$m_{0y} k_y^2 + m_{2x} k_x^4 + m_{2y} k_y^4$, where μ is the chemical potential. The SOPC term in the Hamiltonian is represented by $(A_x k_x \sigma_y, A_y k_y \sigma_x, A_z k_y \sigma_z) s_x$. It would be expected that the SOPC is strongest near the topological band inversion due to s_x , which involves the mixing of two orbitals. The last term is the Zeeman term, where \mathbf{B} is set along in-plane directions and *g*-factor is set to be 2.

In a thin-film structure, the interlayer coupling would make the system to become metallic even without doping. As an illustration, we plot the energy bands of the bilayer 2M-WS₂ in Fig. 1(c). It should be noted that the SOPC arising from the *p*-, *d*-band inversion and strong spin-orbit coupling still exhibits in this case. We also construct a $\mathbf{k} \cdot \mathbf{p}$ Hamiltonian of a bilayer 2M-WS₂ by coupling two copies of monolayer Hamiltonian with interlayer couplings. The detailed form of this bilayer Hamiltonian and model parameters obtained from fitting the first principle calculated bands are listed in Supplementary Sec. I.

In the superconducting state, we can describe the system with Bogoliubov-de Gennes (BdG) Hamiltonian:

$$H_{BdG}(\mathbf{k}) = \begin{pmatrix} H_0(\mathbf{k}) & \Delta(\mathbf{k}) i \sigma_y \\ (\Delta(\mathbf{k}) i \sigma_y)^\dagger & -H_0^*(-\mathbf{k}) \end{pmatrix}. \quad (2)$$

where $H_0(\mathbf{k})$ is the normal state Hamiltonian, $\Delta(\mathbf{k})$ denotes the superconducting order parameters. Later, we will classify all possible pairings according to the irreducible representations of C_{2h} .

Spin-triplet correlations.— Let us first consider the simplest case with $\Delta(\mathbf{k}) = \Delta$ and $H_0(\mathbf{k})$ takes the form of Eq. (1). We would show that due to the presence of strong SOPC, the spin-triplet pairing correlation in Green's function is finite even with this uniform s-wave pairing order parameter.

The Green's function is a convenient way to capture the superconducting properties, which can be expressed with

$$G_{\lambda\mu}(\mathbf{k}, \tau) = -\langle T_\tau \{ c_{\mathbf{k},\lambda}(\tau) c_{\mathbf{k},\mu}^\dagger(0) \} \rangle, \quad (3)$$

$$F_{\lambda\mu}(\mathbf{k}, \tau) = \langle T_\tau \{ c_{\mathbf{k},\lambda}(\tau) c_{-\mathbf{k},\mu}(0) \} \rangle. \quad (4)$$

Here, τ is imaginary time, λ, μ are internal degrees of freedom, T_τ is the time-ordering operator. We can rewrite the Green's function in the Matsubara frequency space: $G_{\lambda\mu}(\mathbf{k}, i\omega_n) = \int_0^\beta d\tau e^{i\omega_n \tau} G_{\lambda\mu}(\mathbf{k}, \tau)$ and $F_{\lambda\mu}(\mathbf{k}, i\omega_n) = \int_0^\beta d\tau e^{i\omega_n \tau} F_{\lambda\mu}(\mathbf{k}, \tau)$. The latter $F_{\lambda\mu}(\mathbf{k}, i\omega_n)$ represents the pairing correlations we refer, which captures the properties of Cooper pairs. These two Green's functions are related to the Gor'kov Green's function as

$$\mathcal{G}(\mathbf{k}, i\omega_n) = \begin{pmatrix} G(\mathbf{k}, i\omega_n) & -F(\mathbf{k}, i\omega_n) \\ -F^\dagger(\mathbf{k}, i\omega_n) & -G^T(-\mathbf{k}, -i\omega_n) \end{pmatrix}. \quad (5)$$

The Gor'kov Green's function can be calculated as $\mathcal{G}(\mathbf{k}, i\omega_n) = (i\omega_n - H_{BdG}(\mathbf{k}))^{-1}$. Insert the BdG Hamiltonian and after some massage, we can parameterize the

TABLE I. Classifications of possible time-reversal-invariant intralayer pairings according to the irreducible representations (IRs) of C_{2h} point group for a bilayer 2M-WS₂. Here the triplet \mathbf{d} -vector is along the direction of SOPC, i.e., $\mathbf{d}(\mathbf{k}) = (A_y k_y, A_x k_x, A_z k_y)$ and $\hat{\mathbf{d}}(\mathbf{k}) = \mathbf{d}(\mathbf{k})/|\mathbf{d}(\mathbf{k})|$.

IRs	A_g	A_u	B_u
$I = s_z$	+	-	-
$C_{2y} = i s_z \sigma_y$	+	+	-
Spin-singlet	s_0, s_z	None	s_x
Spin-triplet	$s_x \hat{\mathbf{d}}(\mathbf{k}) \cdot \boldsymbol{\sigma}$	$s_y \sigma_x, s_y \sigma_z$	$s_y \sigma_y, \hat{\mathbf{d}}(\mathbf{k}) \cdot \boldsymbol{\sigma}$

pairing correlation as

$$F(\mathbf{k}, i\omega_n) = \Delta [C_1(\mathbf{k}, i\omega_n) + C_2(\mathbf{k}, i\omega_n) s_x \mathbf{d}(\mathbf{k}) \cdot \boldsymbol{\sigma}] i\sigma_y, \quad (6)$$

where the detailed expressions of coefficients $C_1(\mathbf{k}, i\omega_n)$ and $C_2(\mathbf{k}, i\omega_n)$ are presented in Supplementary Sec. II.

Notably, it can be seen that there is a triplet component in the pairing correlation, where we find that the triplet d -vector is the SOPC vector (see Supplementary Sec. II):

$$\mathbf{d}(\mathbf{k}) \approx (A_y k_y, A_x k_x, A_z k_y). \quad (7)$$

The structure of the correlation $F(\mathbf{k}, i\omega_n)$ indicates that due to the presence of SOPC, the intra-orbital spin-singlet pairing and the interorbital spin-triplet pairing are mixed with each other.

Symmetry analysis.—From the pairing correlation $F(\mathbf{k}, i\omega)$ in Eq. (6), we can see that the intra-orbital spin-singlet pairing and the inter-orbital spin-triplet pairing in general would mix with each other. Next, let us show this from the symmetry point of view. The pairing order parameter can be classified according to the transformation properties of the pairing matrix $\Delta(\mathbf{k})$ under the group generators of C_{2h} including an inversion operator $I = s_z$ and a two-fold rotation $C_{2y} = i s_z \sigma_y$.

We summarize all possible time-reversal-invariant intralayer pairings C_{2h} in Table I according to the irreducible representations of C_{2h} . The nontrivial A_u -pairing includes two inter-orbital spin-triplet pairings $\Delta_{A_{u,1}} = s_y \sigma_x$ and $\Delta_{A_{u,2}} = s_y \sigma_z$. The nontrivial B_u -pairing includes a spin-singlet pair $\Delta_{B_{u,1}} = s_x$ and triplet pairings $\Delta_{B_{u,2}} = s_y \sigma_y$ and $\Delta_{B_{u,3}} = \hat{\mathbf{d}}(\mathbf{k}) \cdot \boldsymbol{\sigma}$. As we found all the nontrivial A_u - and B_u -pairings lead to a divergent B_{c2} when $T \rightarrow 0$, which are unlikely in the experiment. We would thus focus on A_g -pairing only.

The A_g -pairing allows an intra-orbital spin-singlet pairing, and particularly also allows an inter-orbital spin-singlet pairing $\Delta_{A_{g,2}} = s_x \hat{\mathbf{d}}(\mathbf{k}) \cdot \boldsymbol{\sigma}$. Similar to the non-centrosymmetric superconductors case [4], the triplet $\hat{\mathbf{d}}(\mathbf{k})$ -vector should be parallel to the spin-orbit coupling vector in order to save free energy. As these two pairings belong to the same irreducible representation, they generally would mix with each other, being consistent with

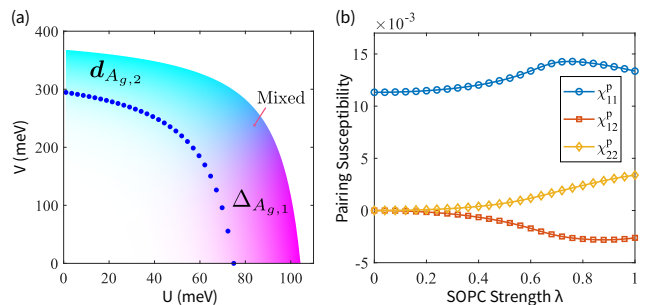


FIG. 2. (a) shows the superconducting phase diagram with intra-orbital spin-singlet pairing $\Delta_{A_{g,1}}$ and inter-orbital spin-triplet pairing $\mathbf{d}_{A_{g,2}}$. The blue dots denote the regime with critical temperature of 7.6 K. (b) shows the pairing susceptibility of χ^p as a function of SOPC strength λ , where χ_{11}^p and χ_{22}^p represent the pairing susceptibility of the pairing $\Delta_{A_{g,1}}$ and $\mathbf{d}_{A_{g,2}}$, respectively. χ_{12}^p represents the mixed pairing susceptibility between the pairing $\Delta_{A_{g,1}}$ and $\mathbf{d}_{A_{g,2}}$.

the pairing correlations shown previously (Eq. (6)). Our analysis clearly shows the discussion of spin-singlet and spin-triplet pairing proposed in noncentrosymmetric superconductors [1–4] can be extended even in centrosymmetric superconductors.

Superconducting phase diagrams and pairing susceptibility.—To show how the mixing strength is affected by interaction strength and the SOPC strength, we study the superconducting phase diagram of A_g pairing and show how these two pairings are stabilized under various SOPC strength.

The superconducting phase diagram can be obtained by solving the linearized gap equation. For simplicity, we neglect s_z in $A_{g,1}$, which only represents a pairing gap difference between two orbitals. Now we study the pairing instability of A_g representation with a conventional intra-orbital spin-singlet pairing $\Delta_{A_{g,1}} = s_0$ and an inter-orbital spin-triplet pairing $\Delta_{A_{g,2}} \equiv \mathbf{d}_{A_{g,2}} = s_x \hat{\mathbf{d}} \cdot \boldsymbol{\sigma}$. The corresponding linearized equation is written as

$$\det \left[\begin{pmatrix} \frac{1}{U} - \chi_{11}^p(T_c) & -\chi_{12}^p(T_c) \\ -\chi_{21}^p(T_c) & \frac{1}{V} - \chi_{22}^p(T_c) \end{pmatrix} \right] = 0, \quad (8)$$

where $\chi_{mm'}^p$ denotes the pairing susceptibility: $\chi_{mm'}^p = -\frac{1}{\beta} \sum_{\mathbf{n}, \mathbf{k}} \text{Tr} [G_e(\mathbf{k}, i\omega_n) (\Delta_{\Gamma, m} i\sigma_y) G_h(\mathbf{k}, i\omega_n) (\Delta_{\Gamma, m'} i\sigma_y)^\dagger]$. Here, the single particle electron Green's function $G_e(\mathbf{k}, i\omega_n) = (i\omega_n - H_0(\mathbf{k}))^{-1}$ and hole Green's function $G_h(\mathbf{k}, i\omega_n) = (i\omega_n + H_0^*(-\mathbf{k}))^{-1}$, where $H_0(\mathbf{k})$ is the normal Hamiltonian. The pairing susceptibility can be calculated numerically in band basis. We label the intra-orbital interaction strength and inter-orbital interaction strength as U and V respectively.

Figure 2(a) shows the calculated superconducting phase diagram with intra-orbital spin-singlet pairing $\Delta_{A_{g,1}}$ and inter-orbital spin-triplet pairing $\mathbf{d}_{A_{g,2}}$. The critical temperature is determined by solving Eq. (8) and the mixing (represented by the color in Fig. 2(a))

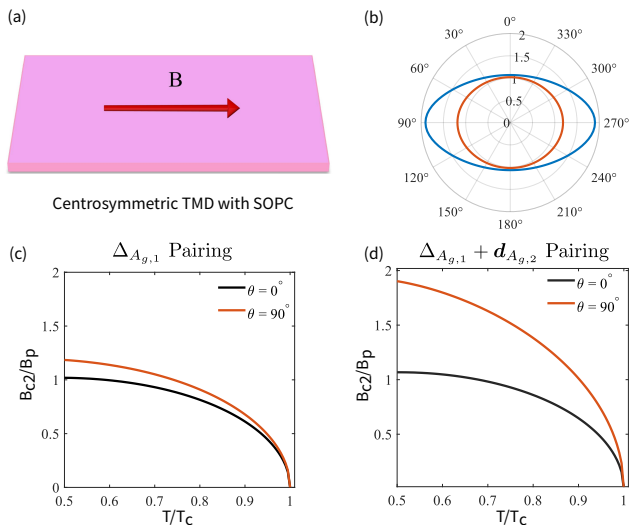


FIG. 3. (a) schematically shows the a centrosymmetric TMD, such as the 2M-WS₂ thin film, in the presence of in-plane fields. (b) shows the angular dependence of in-plane upper critical fields for a bilayer 2M-WS₂ with purely $\Delta_{A_{g1}}$ pairing (red) and $\Delta_{A_{g1}} + \mathbf{d}_{A_{g2}}$ mixed pairing (blue), where the radius shows the value of B_{c2}/B_p , and the temperature is fixed at $T = 0.5T_c$. (c) and (d) The calculated B_{c2}/B_p versus T/T_c curve for the 2M-WS₂ with the in-plane magnetic field direction applied along $\theta = 0^\circ$ and $\theta = 90^\circ$, respectively. Here, we have adopted the interaction parameters $(U, V) = (75, 0)$ meV for $\Delta_{A_{g1}}$ pairing and $(U, V) = (10.7, 288)$ meV for $\Delta_{A_{g1}} + \mathbf{d}_{A_{g2}}$ pairing.

is obtained from the eigenvectors of Eq. (8). As expected, the conventional intra-orbital spin-singlet $A_{g,1}$ pairing is more favorable when the intra-orbital interaction strength U is stronger, while the inter-orbital spin-triplet $A_{g,2}$ pairing is more favorable when the inter-orbital interaction strength V is stronger. At certain (U, V) regime, a prominent mixed region can also be seen, as highlighted in Fig. 2(a). This mixing is allowed by symmetries since both pairings belong to A_g representation. As discussed in the pairing correlations (Eq. 6), such mixing is induced by the SOPC. A purely $\mathbf{d}_{A_{g2}}$ pairing region can also be seen in Fig. 2(a).

In Fig. 2(b), we display the pairing susceptibility of χ^p as a function of SOPC strength λ , where the SOPC coefficients are scaled as λA_j . It can be seen that the mixing vanishes ($\chi_{12}^p = 0$) when there is no SOPC ($\lambda = 0$). We also noted the magnitude of the pairing susceptibility χ_{12}^p increases with the SOPC strength. It means that the spin-triplet pairing $\mathbf{d}_{A_{g2}}$ is more favorable when the SOPC is stronger. The enhancement of $\mathbf{d}_{A_{g2}}$ pairing stems from the fact that $\mathbf{d}_{A_{g2}}$ pairing is inter-orbital pairing and the SOPC can introduce the orbital mixing. In contrast, as shown in Fig. 2(b), the pairing susceptibility of conventional spin-singlet pairing $\Delta_{A_{g,1}}$ is relatively insensitive to the SOPC strength.

In-plane upper critical fields. As we discussed, the symmetry allows a mixed of $\Delta_{A_{g1}}$ pairing and $\mathbf{d}_{A_{g2}}$ pairing. In this section, we show that how the in-plane upper critical fields (Fig. 3(a)) are changed in the presence of the additional $\mathbf{d}_{A_{g2}}$ pairing mixing. In this case, we need to solve the linearized gap equation Eq. (8) with replacing the pairing susceptibilities $\chi^p(T)$ with ones of finite fields $\chi^p(B, T)$. i.e.,

$$\det \left[\begin{pmatrix} \frac{1}{U} - \chi_{11}^p(B, T) & -\chi_{12}^p(B, T) \\ -\chi_{21}^p(B, T) & \frac{1}{V} - \chi_{22}^p(B, T) \end{pmatrix} \right] = 0. \quad (9)$$

The results are summarized in Fig. 3. Fig. 3(b) shows the angular dependence of B_{c2}/B_p of a purely spin-singlet state $\Delta_{A_{g1}}$ and spin-singlet (blue) and spin-triplet mixed state (red). It clearly shows that the enhancement and anisotropic ratio of B_{c2} can be enhanced by the mixing of $\mathbf{d}_{A_{g2}}$ pairing. In Fig. 3(c) and Fig. 3(d), the calculated in-plane critical magnetic fields as a function of temperature are plotted for a purely $\Delta_{A_{g1}}$ pairing and $\Delta_{A_{g1}} + \mathbf{d}_{A_{g2}}$. Consistently, we find the enhancement for the $\Delta_{A_{g1}} + \mathbf{d}_{A_{g2}}$ pairing is larger than a purely $\Delta_{A_{g1}}$ pairing. More importantly, the sizable enhancement $B_{c2} \approx 2B_p$ for fields along $\theta = 90^\circ$ suggested by $\Delta_{A_{g1}} + \mathbf{d}_{A_{g2}}$ pairing is very close to the experimental data of 2M-WS₂ thin-film [18].

The $\mathbf{d}_{A_{g2}}$ -pairing enhances the critical magnetic fields is understandable, because it is a spin-triplet pairing which can induce equal-spin cooper pairs and save magnetic energy in a superconducting state. However, this spin-triplet pairing would not lead to a divergent B -fields as $T \rightarrow 0$ as a usual spin-triplet pairing even in the absence of orbital effects. This is because the direction of spin-triplet \mathbf{d} -vector is not fixed within the momentum space for this centrosymmetric system. It is significantly different from 2H-type superconducting TMDs, where the favorable spin-triplet \mathbf{d} -vector is pinned along out of plane direction [12, 14].

Andreev reflection— To further verify our theory, we propose to attach a ferromagnetic lead to these centrosymmetric superconducting TMDs and calculate for the Andreev reflection.

We model the ferromagnetic lead with a square lattice. For simplicity, we use a monolayer $\mathbf{k} \cdot \mathbf{p}$ Hamiltonian in tight-binding limit. Using the Fisher-Lee trick [28, 29], the scattering matrix is given by

$$S = \begin{pmatrix} r_{ee} & r_{eh} \\ r_{he} & r_{hh} \end{pmatrix} = -I + i\Gamma^{1/2} G^R(E) \Gamma^{1/2}, \quad (10)$$

where r_{ee}, r_{he} are the electron and Andreev reflection matrix respectively. $\Gamma = i(\Sigma - \Sigma^\dagger)$ is the broadening function, Σ is the self-energy, and $G^R(E)$ is the total (retarded) Green's function. The conductance is then given by (c.f. [30])

$$G(E) = \frac{e^2}{h} \text{Tr} \left[I - r_{ee}^\dagger r_{ee} + r_{he}^\dagger r_{he} \right]. \quad (11)$$

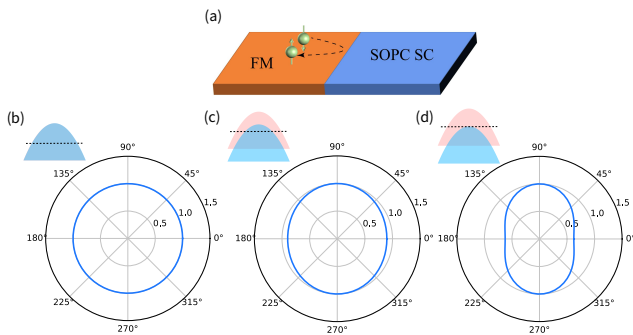


FIG. 4. (a) The schematic plot of a ferromagnet metal/SOPC superconductor (SC) tunneling junction. The Andreev reflection process is highlighted on the plot. (b)-(d) The angular dependence of in-gap normalized tunnel conductance G , where the angle represents the in-plane magnetization direction. From left to right, we illustrate the major spin and minor spin population in each case. It can be clearly seen that the Andreev reflection amplitude exhibits a two-fold feature when m is finite in the ferromagnetic metal lead. The two-fold anisotropic feature will become more salient when ferromagnetic metal lead is close to a half-metal in, in which almost only half of the spin population is occupied.

Fig. 4(b)-(d) show the in-gap conductance at different magnetization amplitude. Similar to Fig. 3, when rotating the polarization direction of the ferromagnetic lead, the in-gap Andreev reflection exhibits anisotropy with a two-fold symmetry, showing suppression at angles of $\theta = 0^\circ, 180^\circ$. This is due to the triplet pairing correlations induced by the strong SOPC. In 2M-WS₂, the triplet \mathbf{d} -vector at the Fermi surface is approximately parallel to the x -axis. This favours equal-spin triplet pairing in y -direction. As a result, when the magnetization angle is at 0° , Andreev reflection of equal-spin holes is suppressed [20]. In contrast, approaching to 90° , equal-spin hole can be reflected. The same argument repeats for 180° and 270° . The results should be similar in other SOPC superconductors since it is mostly controlled by the triplet \mathbf{d} -vector which is proportional to the SOPC vector. We also include a similar calculation for 1T'-WTe₂ in Supplementary Sec. IV.

Conclusions.—In conclusion, we have established a self-consistent mean-field theory to demonstrate singlet-triplet mixed state induced by the SOPC in centrosymmetric superconductors. In particular, our finding explains the observed enhancement of B_{c2} with a large anisotropic ratio in 2M-WS₂ thin film. Furthermore, we find anisotropic in-gap Andreev reflection amplitudes at the FM/SOPC superconductor tunneling junction with respect to the magnetization direction of the FM lead. The result can be experimentally tested to verify spin-triplet pairing in general SOPC superconductor. Our theory generally applies to other similar centrosymmetric superconducting TMDs, such as 1T'-WTe₂, 1T'-WS₂.

Acknowledgments.—Tsz Fung Heung and Yip Chun

Wong sincerely express their heartfelt appreciation for the invaluable insights and guidance offered by Yingming Xie, Benjamin T. Zhou and K.T. Law. They also extend their sincere gratitude for the DFT calculation data of 2M-WS₂ provided by Xue-Jian Gao.

* These two authors contributed equally

- [1] L. P. Gor'kov and E. I. Rashba, *Phys. Rev. Lett.* **87**, 037004 (2001).
- [2] M. Smidman, M. B. Salamon, H. Q. Yuan, and D. F. Agterberg, *Reports on Progress in Physics* **80**, 036501 (2017).
- [3] E. Bauer and M. Sigrist, *Non-centrosymmetric superconductors: introduction and overview*, Vol. 847 (Springer Science & Business Media, 2012).
- [4] P. A. Frigeri, D. F. Agterberg, A. Koga, and M. Sigrist, *Phys. Rev. Lett.* **92**, 097001 (2004).
- [5] J. M. Lu, O. Zheliuk, I. Leermakers, N. F. Q. Yuan, U. Zeitler, K. T. Law, and J. T. Ye, *Science* **350**, 1353 (2015).
- [6] X. Xi, Z. Wang, W. Zhao, J.-H. Park, K. T. Law, H. Berger, L. Forró, J. Shan, and K. F. Mak, *Nature Physics* **12**, 139 (2016).
- [7] Y. Saito, Y. Nakamura, M. S. Bahramy, Y. Kohama, J. Ye, Y. Kasahara, Y. Nakagawa, M. Onga, M. Tokunaga, T. Nojima, Y. Yanase, and Y. Iwasa, *Nature Physics* **12**, 144 (2016).
- [8] S. C. de la Barrera, M. R. Sinko, D. P. Gopalan, N. Sivasdas, K. L. Seyler, K. Watanabe, T. Taniguchi, A. W. Tsen, X. Xu, D. Xiao, and B. M. Hunt, *Nature Communications* **9**, 1427 (2018).
- [9] J. Lu, O. Zheliuk, Q. Chen, I. Leermakers, N. E. Hussey, U. Zeitler, and J. Ye, *Proceedings of the National Academy of Sciences* **115**, 3551 (2018).
- [10] Y. Xing, K. Zhao, P. Shan, F. Zheng, Y. Zhang, H. Fu, Y. Liu, M. Tian, C. Xi, H. Liu, J. Feng, X. Lin, S. Ji, X. Chen, Q.-K. Xue, and J. Wang, *Nano Letters* **17**, 6802 (2017).
- [11] E. Sohn, X. Xi, W.-Y. He, S. Jiang, Z. Wang, K. Kang, J.-H. Park, H. Berger, L. Forró, K. T. Law, J. Shan, and K. F. Mak, *Nature Materials* **17**, 504 (2018).
- [12] B. T. Zhou, N. F. Q. Yuan, H.-L. Jiang, and K. T. Law, *Phys. Rev. B* **93**, 180501 (2016).
- [13] W.-Y. He, B. T. Zhou, J. J. He, N. F. Q. Yuan, T. Zhang, and K. T. Law, *Communications Physics* **1**, 40 (2018).
- [14] Y. Xie, B. T. Zhou, T. K. Ng, and K. T. Law, *Phys. Rev. Research* **2**, 013026 (2020).
- [15] D. Wickramaratne, S. Khmelevskiy, D. F. Agterberg, and I. I. Mazin, *Phys. Rev. X* **10**, 041003 (2020).
- [16] V. Fatemi, S. Wu, Y. Cao, L. Bretheau, Q. D. Gibson, K. Watanabe, T. Taniguchi, R. J. Cava, and P. Jarillo-Herrero, *Science* **362**, 926 (2018).
- [17] E. Sajadi, T. Palomaki, Z. Fei, W. Zhao, P. Bement, C. Olsen, S. Luescher, X. Xu, J. A. Folk, and D. H. Cobden, *Science* **362**, 922 (2018).
- [18] E. Zhang, Y.-M. Xie, Y. Fang, J. Zhang, X. Xu, Y.-C. Zou, P. Leng, X.-J. Gao, Y. Zhang, L. Ai, Y. Zhang, Z. Jia, S. Liu, J. Yan, W. Zhao, S. J. Haigh, X. Kou, J. Yang, F. Huang, K. T. Law, F. Xiu, and S. Dong, *Nature Physics* **19**, 106 (2023).

- [19] X. Song, R. Singha, G. Cheng, Y.-W. Yeh, F. Kamm, J. F. Khoury, F. Pielhofer, P. E. Batson, N. Yao, and L. M. Schoop, arXiv e-prints , arXiv:2206.01648 (2022), arXiv:2206.01648 [cond-mat.mtrl-sci].
- [20] Y. Liu, Y. Xu, J. Sun, C. Liu, Y. Liu, C. Wang, Z. Zhang, K. Gu, Y. Tang, C. Ding, H. Liu, H. Yao, X. Lin, L. Wang, Q.-K. Xue, and J. Wang, *Nano Letters* **20**, 5728 (2020).
- [21] J. Falson, Y. Xu, M. Liao, Y. Zang, K. Zhu, C. Wang, Z. Zhang, H. Liu, W. Duan, K. He, H. Liu, J. H. Smet, D. Zhang, and Q.-K. Xue, *Science* **367**, 1454 (2020), <https://www.science.org/doi/pdf/10.1126/science.aax3873>.
- [22] X. Qian, J. Liu, L. Fu, and J. Li, *Science* **346**, 1344 (2014).
- [23] L. Muechler, A. Alexandradinata, T. Neupert, and R. Car, *Phys. Rev. X* **6**, 041069 (2016).
- [24] S. Tang, C. Zhang, D. Wong, Z. Pedramrazi, H.-Z. Tsai, C. Jia, B. Moritz, M. Claassen, H. Ryu, S. Kahn, J. Jiang, H. Yan, M. Hashimoto, D. Lu, R. G. Moore, C.-C. Hwang, C. Hwang, Z. Hussain, Y. Chen, M. M. Ugeda, Z. Liu, X. Xie, T. P. Devereaux, M. F. Crommie, S.-K. Mo, and Z.-X. Shen, *Nature Physics* **13**, 683 (2017).
- [25] Z. Fei, T. Palomaki, S. Wu, W. Zhao, X. Cai, B. Sun, P. Nguyen, J. Finney, X. Xu, and D. H. Cobden, *Nature Physics* **13**, 677 (2017).
- [26] S. Wu, V. Fatemi, Q. D. Gibson, K. Watanabe, T. Taniguchi, R. J. Cava, and P. Jarillo-Herrero, *Science* **359**, 76 (2018).
- [27] Y.-M. Xie, B. T. Zhou, and K. T. Law, *Phys. Rev. Lett.* **125**, 107001 (2020).
- [28] P. A. Lee and D. S. Fisher, *Physical Review Letters* **47**, 882 (1981).
- [29] D. S. Fisher and P. A. Lee, *Physical Review B* **23**, 6851 (1981).
- [30] S. Manna, P. Wei, Y. Xie, K. T. Law, P. A. Lee, and J. S. Moodera, *Proceedings of the National Academy of Sciences* **117**, 8775 (2020), <https://www.pnas.org/doi/pdf/10.1073/pnas.1919753117>.

Supplementary Material for “Spin-orbital-parity coupling induced singlet-triplet mixed state in centrosymmetric superconducting transition metal dichagenides”

Tsz Fung Heung,^{*,1} Yip Chun Wong,^{*,1}

¹*Department of Physics, Hong Kong University of Science and Technology, Clear Water Water Bay, Hong Kong, China*

I. EFFECTIVE $\mathbf{k} \cdot \mathbf{p}$ HAMILTONIANS

The crystal structure of 2M-WS₂ respects to point group C_{2h} . The generators are an inversion symmetry and a two-fold symmetry along y axis. From the results of first principle calculation, the bands near Fermi energy are dominant by the orbitals $|S, A_u\rangle$, $|W, B_g\rangle$. Here, A_u corresponds to a p -wave-like orbit, while B_g corresponds to a d -wave-like orbit. As a result, the representations of the generators can be written as $C_{2y} = i\sigma_y s_z \tau_x$ and $I = s_z \tau_x$, where Pauli matrices τ , s , σ operate on layer, orbital, spin space respectively.

Based on these symmetry generators, a $\mathbf{k} \cdot \mathbf{p}$ normal Hamiltonian for monolayer 2M-WS₂ dictated by the C_{2h} symmetry is obtained as

$$H_0(\mathbf{k}) = \epsilon(\mathbf{k}) + \mathcal{M}(\mathbf{k})s_z + v(\mathbf{k})k_x s_y + (A_x k_x s_x \sigma_y + A_y k_y s_x \sigma_x + A_z k_y s_x \sigma_z). \quad (S1)$$

where $\epsilon(\mathbf{k}) = t_{0x}k_x^2 + t_{0y}k_y^2 + t_{2x}k_x^4 + t_{2y}k_y^4 - \mu$, $\mathcal{M}(\mathbf{k}) = -\delta + m_{0x}k_x^2 + m_{0y}k_y^2 + m_{2x}k_x^4 + m_{2y}k_y^4$, $v(\mathbf{k}) = v_1 + v_2k_x^2 + v_3k_y^2$. μ is the chemical potential.

By adding the interlayer coupling Hamiltonian, we can construct an effective Hamiltonian for a bilayer 2M-WS₂:

$$H_N(\mathbf{k}) = H_0(\mathbf{k})\tau_0 + H_c(\mathbf{k})\sigma_0 \quad (S2)$$

Here the basis $\psi_{\mathbf{k}} = (\psi_{\mathbf{k},+}, \psi_{\mathbf{k},-})^T$ with $\psi_{\mathbf{k},l} = (c_{\mathbf{k},p,\uparrow,l}, c_{\mathbf{k},p,\downarrow}, c_{\mathbf{k},d,\uparrow,l}, c_{\mathbf{k},d,\downarrow})$, where l is the layer-index and $c_{\mathbf{k},s,\sigma,l}$ is electron annihilation operator with orbit s , spin σ and layer l . The interlayer coupling Hamiltonian $H_c(\mathbf{k})$ is given by

$$H_c(\mathbf{k}) = (B(\mathbf{k}) + C(\mathbf{k})s_z + Dk_x s_y)\tau_x + (\gamma_0 k_x \tau_y + \gamma_1 k_x \tau_y s_z) + \alpha(\mathbf{k})s_x \tau_z + \beta(\mathbf{k})s_y \tau_y, \quad (S3)$$

where $B(\mathbf{k}) = B_0 + B_x k_x^2 + B_y k_y^2$, $C(\mathbf{k}) = C_0 + C_x k_x^2 + C_y k_y^2$, $\alpha(\mathbf{k}) = \alpha_0 + \alpha_x k_x^2 + \alpha_y k_y^2$, $\beta(\mathbf{k}) = \beta_0 + \beta_x k_x^2 + \beta_y k_y^2$. For simplicity, only the spin-independent interlayer coupling is considered.

The value of model parameters, which are obtained from fitting the band structures of the bilayer 2M-WS₂, are listed in the Supplementary Table S1. The chemical potential μ is set to be 90 meV for the main text Fig. 1.

TABLE S1. List of model parameters (in units of meV) obtained from fitting the band structures of the bilayer 2M-WS₂.

t_{0x}	t_{0y}	t_{2x}	t_{2y}	δ	m_{0x}	m_{0y}	m_{2x}
-3.21	67.0991	-14.37	-6.19	-88.80	-117.99	-190.44	-0.70
m_{2y}	v_1	v_2	v_3	A_x	A_y	A_z	B_0
-204.65	110.37	-18.37	-203.73	20.00	101.00	86.00	131.75
B_x	B_y	C_0	C_x	C_y	α_0	α_x	α_y
-25.45	52.66	42.53	-0.34	22.88	-32.02	-3.87	99.16
β_0	β_x	β_y	D	γ_0	γ_1		
-5.39	-11.53	77.81	-112.31	63.36	29.21		

II. PAIRING CORRELATIONS

Although we only consider the simplest conventional intra-orbital spin singlet pairing, i.e., $\Delta i\sigma_y$, here we show that the SOPC will induce some interorbital spin-triplet correlations, which also helps to enhance the upper critical field. To show this, we consider the following minimal model for a SOPC superconductor:

$$H_N(\mathbf{k}) = \epsilon_{\mathbf{k}} + \mathcal{M}_{\mathbf{k}}s_z + vk_x s_y + (A_x k_x s_x \sigma_y + A_y k_y s_x \sigma_x + A_z k_y s_x \sigma_z) + u_B \mathbf{B} \cdot \boldsymbol{\sigma}, \quad (S4)$$

and the BdG Hamiltonian is

$$H_{BdG}(\mathbf{k}) = \begin{pmatrix} H_N(\mathbf{k}, \mathbf{B}) & \Delta i\sigma_y \\ (\Delta i\sigma_y)^\dagger & -H_N^*(-\mathbf{k}, \mathbf{B}) \end{pmatrix} \quad (S5)$$

Let us identify the superconducting properties in terms of Green's function.

$$G_{\lambda\mu}(\mathbf{k}, \tau) = -\langle T_\tau \{c_{\mathbf{k},\lambda}(\tau)c_{\mathbf{k},\mu}^\dagger(0)\} \rangle, \quad (S6)$$

$$F_{\lambda\mu}(\mathbf{k}, \tau) = \langle T_\tau \{c_{\mathbf{k},\lambda}(\tau)c_{-\mathbf{k},\mu}(0)\} \rangle. \quad (S7)$$

We can rewrite the Green's function in the Matsubara frequency space: $G_{\lambda\mu}(\mathbf{k}, i\omega_n) = \int_0^\beta d\tau e^{i\omega_n\tau} G_{\lambda\mu}(\mathbf{k}, \tau)$ and $F_{\lambda\mu}(\mathbf{k}, i\omega_n) = \int_0^\beta d\tau e^{i\omega_n\tau} F_{\lambda\mu}(\mathbf{k}, \tau)$. The latter $F_{\lambda\mu}(\mathbf{k}, i\omega_n)$ represents the pairing correlations we refer. These two Green's functions are related to the Gor'kov Green's function as

$$\mathcal{G}(\mathbf{k}, i\omega_n) = (i\omega_n - H_{BdG}(\mathbf{k}))^{-1} = \begin{pmatrix} G(\mathbf{k}, i\omega_n) & -F(\mathbf{k}, i\omega_n) \\ -F^\dagger(\mathbf{k}, i\omega_n) & -G^T(-\mathbf{k}, -i\omega_n) \end{pmatrix}. \quad (S8)$$

Substitute the BdG Hamiltonian into Eq. (S5) and after some massage, we can parameterize the pairing correlation as

$$F(\mathbf{k}, i\omega_n) = \Delta[\hat{C}_1(\mathbf{k}, i\omega_n) + \hat{C}_2(\mathbf{k}, i\omega_n)s_x \mathbf{d}(\mathbf{k}) \cdot \boldsymbol{\sigma}]i\sigma_y \quad (S9)$$

with the coefficients

$$\hat{C}_1(\mathbf{k}, i\omega_n) = \frac{1}{Q(\mathbf{k}, \omega_n)} [-D(\mathbf{k}, \omega_n) + 2\epsilon_{\mathbf{k}} M_{\mathbf{k}} s_z + 2\epsilon_{\mathbf{k}} v k_x s_y], \quad (S10)$$

$$\hat{C}_2(\mathbf{k}, i\omega_n) = \frac{2\epsilon_{\mathbf{k}}}{Q(\mathbf{k}, \omega_n)}, \quad (S11)$$

$$Q(\mathbf{k}, \omega_n) = 4\epsilon_{\mathbf{k}}^2 (v^2 k_x^2 + |\mathbf{A}\mathbf{k}|^2 + M_{\mathbf{k}}^2) - D(\mathbf{k}, \omega_n)^2, \quad (S12)$$

$$D(\mathbf{k}, \omega_n) = \omega_n^2 + \epsilon_{\mathbf{k}}^2 + M_{\mathbf{k}}^2 + v^2 k_x^2 + |\mathbf{A}\mathbf{k}|^2 + \Delta^2, \quad (S13)$$

where the SOPC vector $\mathbf{A}\mathbf{k} \equiv (A_y k_y, A_x k_x, A_z k_y)$. Importantly, the triplet vector is directly related to the SOPC:

$$\mathbf{d}(\mathbf{k}) \approx (A_y k_y, A_x k_x, A_z k_y), \quad (S14)$$

where we have ignore the $O(\mathbf{k}^2)$ terms. Therefore, it can be seen that due to the presence of SOPC, the intraorbital spin-singlet pairing and the interorbital spin-triplet pairing are mixed with each other.

III. THE EVALUATION OF PAIRING SUSCEPTIBILITY IN BAND BASIS

In practice, it is more convenient to evaluate the pairing susceptibility in band basis. Specifically, we can write the pairing susceptibility $\chi_{\Gamma, mm'}^p$ as

$$\begin{aligned} \chi_{\Gamma, mm'}^p &= -\frac{1}{\beta} \sum_{n, \mathbf{p}} \text{Tr}[G_e(\mathbf{p}, i\omega_n)(\Delta_{\Gamma, m} i\sigma_y)G_h(\mathbf{p}, i\omega_n)(\Delta_{\Gamma, m'} i\sigma_y)^\dagger] \\ &= \int \frac{d^2 \mathbf{p}}{(2\pi)^2} \sum_{a, b} O_{a, b}^{\Gamma m}(\mathbf{p}) O_{a, b}^{\Gamma m' \dagger}(\mathbf{p}) \frac{1 - f(E_a(\mathbf{p})) - f(E_b(-\mathbf{p}))}{E_a(\mathbf{p}) + E_b(-\mathbf{p})}. \end{aligned} \quad (S15)$$

Here, the single particle electron Green's function $G_e(\mathbf{p}, i\omega_n) = (i\omega_n - H_0(\mathbf{p}))^{-1}$ and hole Green's function $G_h(\mathbf{p}, i\omega_n) = (i\omega_n + H_0^*(-\mathbf{p}))^{-1}$, the overlap function $O_{a, b}^{\Gamma m}(\mathbf{p}) = \langle u_{a, \mathbf{p}} | \Delta_{\Gamma, m} i\sigma_y | \nu_{b, -\mathbf{p}} \rangle$ with $|u_{a, \mathbf{p}}\rangle, |\nu_{b, \mathbf{p}}\rangle$ being eigenvectors of $H_0(\mathbf{p})$ satisfying $H_0(\mathbf{p}) |u_{a, \mathbf{p}}\rangle = E_a(\mathbf{p}) |u_{a, \mathbf{p}}\rangle$, $H_0^*(-\mathbf{p}) |\nu_{b, \mathbf{p}}\rangle = E_b(\mathbf{p}) |\nu_{b, \mathbf{p}}\rangle$, a, b are the band indices.

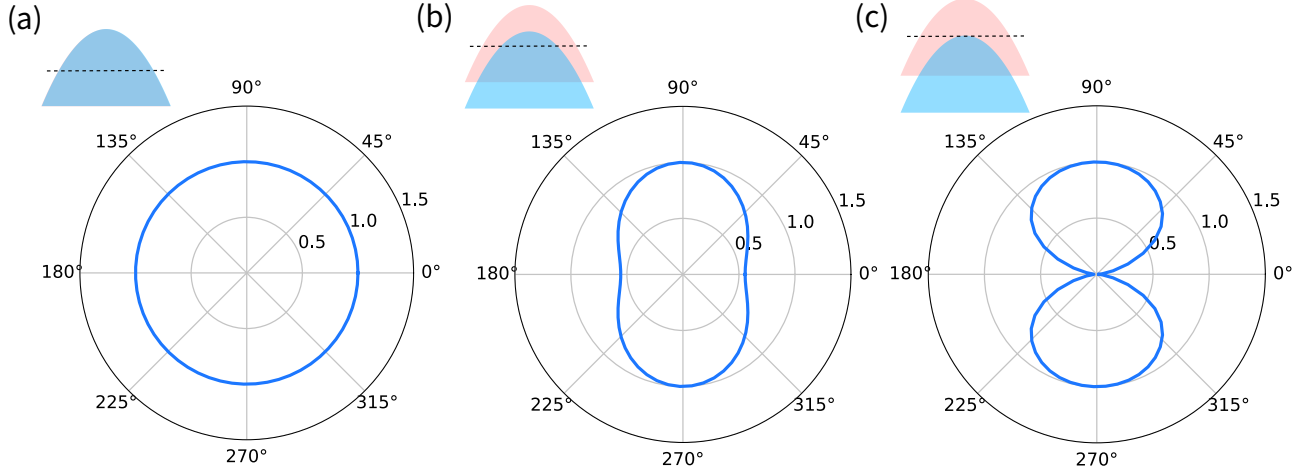


FIG. S1. (a)-(c) The angular dependence of in-gap normalized tunnel conductance G , where the angle represents the in-plane magnetization direction, in the FM/1T'-WTe₂ SC tunneling junction. We set $|\mathbf{m}|/t_{1p} = 0, 0.6, 0.8$ in (a)-(c), respectively. The major spin and minor spin population are illustrated in each case. Again, it can be clearly seen that the Andreev reflection amplitude exhibits a two-fold feature when the magnetization amplitude \mathbf{m} is finite in the ferromagnetic metal lead. The two-fold anisotropic feature becomes significantly more salient when ferromagnetic metal lead is close to a half-metal in (c).

IV. TWO-FOLD ANDREEV REFLECTION AMPLITUDE IN FM/SOPC SC JUNCTION

In this section, we present details of the tight-binding model used to study the tunneling spectrum in Fig. 4 in the main text. In the Nambu basis $(c_{\mathbf{k},p,\uparrow}, c_{\mathbf{k},p,\downarrow}, c_{\mathbf{k},d,\uparrow}, c_{\mathbf{k},d,\downarrow}, c_{-\mathbf{k},p,\uparrow}^\dagger, c_{-\mathbf{k},p,\downarrow}^\dagger, c_{-\mathbf{k},d,\uparrow}^\dagger, c_{-\mathbf{k},d,\downarrow}^\dagger)^T$, where $c_{\mathbf{k},l,\sigma}^\dagger$ ($l = p, d, \sigma = \uparrow, \downarrow$) creates a Bloch state formed by linear combinations of Wannier orbital of character l and spin σ , the momentum-space tight-binding Hamiltonian $\hat{H}_{BdG}^{TB}(\mathbf{k})$ for the SOPC superconductor under the superconducting $\hat{\Delta}$ reads:

$$\hat{H}_{BdG}^{TB}(\mathbf{k}) = \sum_{\mathbf{k},mn} c_{\mathbf{k},m}^\dagger H_{0,mn}^{TB}(\mathbf{k}) c_{\mathbf{k},n} + \Delta (c_{\mathbf{k},p,\uparrow}^\dagger c_{-\mathbf{k},p,\downarrow}^\dagger + c_{\mathbf{k},d,\downarrow}^\dagger c_{-\mathbf{k},d,\uparrow}^\dagger + h.c.). \quad (\text{S16})$$

Here, $m, n = (l, \sigma)$ label the index for different Wannier orbitals with $l = p, d, \sigma = \uparrow, \downarrow$. $H_0^{TB}(\mathbf{k})$ is an 4×4 matrix given by:

$$H_0^{TB}(\mathbf{k}) = \begin{pmatrix} E_p(\mathbf{k}) - \mu & 0 & -iv \sin(k_x a) + A_z \sin(k_y b) & -iA_x \sin(k_x a) + A_y \sin(k_y b) \\ & E_p(\mathbf{k}) - \mu & iA_x \sin(k_x a) + A_y \sin(k_y b) & -iv \sin(k_x a) - A_z \sin(k_y b) \\ & & E_d(\mathbf{k}) - \mu & 0 \\ h.c. & & & E_d(\mathbf{k}) - \mu \end{pmatrix}, \quad (\text{S17})$$

$$\begin{aligned} E_p(\mathbf{k}) &= 2 \{t_{1p} [\cos(k_x a) - 1] + t_{2p} [\cos(k_y b) - 1]\} - \mu_p, \\ E_d(\mathbf{k}) &= 2 \{t_{1d} [\cos(k_x a) - 1] + t_{2d} [\cos(k_y b) - 1] + t'_{2d} [\cos(2k_y b) - 1]\} - \mu_d. \end{aligned} \quad (\text{S18})$$

Here, a monolayer Hamiltonian of 2M-WS₂ is used for simplicity. The parameters above are tabulated in Table S2. It can be verified that $H_0^{TB}(\mathbf{k})$ reduces to the $\mathbf{k} \cdot \mathbf{p}$ model near the Γ -point in Eq. (S1) in the continuum limit $a, b \rightarrow 0$.

The ferromagnetic lead Hamiltonian can be written as

$$H_{\text{lead}} = \sum_{k_x, k_y, s, s'} \psi_{k_x, k_y, s}^\dagger \{ [2t_L \cos(k_x a) + 2t_L \cos(k_y b) - \mu_L] \sigma_{ss'}^0 + \mathbf{m} \cdot \boldsymbol{\sigma}_{ss'} \} \psi_{k_x, k_y, s'} \quad (\text{S19})$$

We can the Fourier transform: $\psi_{m,n,s} = \frac{1}{\sqrt{N}} \sum_{k_x, k_y} e^{-imk_x a - ink_y b} \psi_{k_x, k_y, s}, c_{m,n,p(d),s} = \frac{1}{\sqrt{N}} \sum_{k_x, k_y} e^{-imk_x a - ink_y b} c_{k_x, k_y, p(d),s}$ and change above Hamiltonian as the lattice model. The coupling Hamiltonian between the lead and the SOPC superconductor is written as

$$H_{\text{couple}} = \sum_{m,n,s} -(t_c \psi_{m,n,s}^\dagger c_{m,n,p,s} + t_c \psi_{m,n,s}^\dagger c_{m,n,d,s}) + h.c. \quad (\text{S20})$$

The tunneling spectrum is calculated by the recursive Green's function (c.f. Ref. [S1]):

$$G(E) = \frac{e^2}{h} \text{Tr}[I - r_{ee}^\dagger(E)r_{ee}(E) + r_{he}^\dagger(E)r_{he}(E)]. \quad (\text{S21})$$

Here r_{ee}/r_{he} are the normal reflection/Andreev reflection amplitude respectively. In main text Fig. 4, we set $\mu = 90$ meV, $\Delta_1 = 6$ meV, $t_L = 4|\mathbf{m}|$, $t_c = t_{1p}/3$, and the magnetization vector $\mathbf{m} = |\mathbf{m}|(\cos\theta, \sin\theta, 0)$, and $E = 0$. The magnetization amplitude $|\mathbf{m}|$ for main text Fig. 4(b)-(d) are $|\mathbf{m}| = 0, 0.75, 0.8|t_{1p}|$, respectively.

To show that spin-triplet pairing generally exists in SOPC superconductor, we adopt 1T'-WTe₂ parameters from Ref. [S2] (tabulated in Table. S3) and perform the same calculation. In Fig. S1, we set $\mu = 60$ meV. The other parameters of the lead and the coupling Hamiltonian take the same form as before.

TABLE S2. 2M-WS₂ tight-binding parameters in $H_0^{TB}(\mathbf{k})$ in Eq. (S17) (in units of meV). Lattice constants: $a = 5.71$ Å, $b = 3.23$ Å.

μ_p	μ_d	t_{1p}	t_{2p}	t_{1d}	t_{2d}	t'_{2d}	v	A_x	A_y	A_z
-88.8	88.8	-121.2	-123.34	-114.78	337.84	148.85	110.37	20	101	86

TABLE S3. 1T'-WTe₂ tight-binding parameters in $H_0^{TB}(\mathbf{k})$ in Eq. (S17) (in units of meV). Lattice constants: $a = 6.31$ Å, $b = 3.49$ Å.

μ_p	μ_d	t_{1p}	t_{2p}	t_{1d}	t_{2d}	t'_{2d}	v	A_x	A_y	A_z
-1390	62	626	1517	-60	-387	150	371	27	163	20

* These two authors contributed equally

[S1] S. Manna, P. Wei, Y. Xie, K. T. Law, P. A. Lee, and J. S. Moodera, Proceedings of the National Academy of Sciences **117**, 8775 (2020), <https://www.pnas.org/doi/pdf/10.1073/pnas.1919753117>.

[S2] Y.-M. Xie, B. T. Zhou, and K. T. Law, Phys. Rev. Lett. **125**, 107001 (2020).